ELSEVIER

Physica B 314 (2002) 444–449

PHYSICA B

www.elsevier.com/locate/physb

Probing a single quantum dot by pulsed and continuous microwave radiation

H. Qin[a], J. Truitt[b], D.W. van der Weide[b], R.H. Blick[a,*]

[a] *Center for NanoScience and Sektion Physik, Ludwig-Maximilians-Universität, Geschwister-Scholl-Platz 1, 80539 München, Germany*
[b] *Department of Electrical and Computer Engineering, University of Wisconsin, 1415 Engineering Dr, Madison, WI 53706, USA*

Abstract

Using both picosecond millimeter-wave impulses and continuous microwave radiation, we probe the electronic structure and dynamic response of single-electron tunneling in structured quantum dots, essential for understanding their applications as computational elements, emitters and detectors. Under pulsed microwave radiation, the dot's capacitance is greatly reduced compared to the equilibrium values. In contrast, the dot's capacitance remains constant under continuous microwave radiation. This phenomenological reduction of capacitance stems from the faster pumping of electrons by pulsed microwave excitation as compared to the slow relaxation of electrons.

PACS: 07.57.Hm; 73.23.Hk; 73.21.La

Keywords: Millimeter-wave; Coulomb-blockade; SET; Quantum dots

Structured quantum dots are few-electron systems used not only as models of atoms and molecules but also as building blocks for quantum computers [1] and quantum emitters and detectors of phonons or photons [2–4]. They are usually electrostatically confined by nanometer-sized gates and coupled to leads, enabling transport spectroscopy. Coherent superpositions of covalent molecular states of tunnel-coupled quantum dots have been realized by applying continuous microwaves [5,6]. Pulsed microwaves are desired to control the coherent superposition of molecular states [7], i.e., realizing a quantum bit (qubit). On the other hand, pulsed microwaves are expected to switch qubits for simple quantum computing operations. Characterizations of dynamic responses of electrons in quantum dots to the microwave pulses are thus essential. In fact, time-resolved measurements of Cooper pair tunneling in coupled Josephson junctions by Nakamura et al. [8] have spurred interest in using temporal information to investigate the electron dynamics of dots. Recently, some aspects of electron dynamics have been investigated in single quantum dots using different techniques [9,10]. It was found that excited states can have a relaxation time as long as a few μs, which is attributed to slow spin relaxation processes [10].

*Corresponding author. Tel.: +49-89-2180-3733; fax: +49-89-2180-3182.

E-mail address: robert.blick@physik.uni-muenchen.de (R.H. Blick).

0921-4526/02/$ - see front matter
PII: S0921-4526(01)01382-5

Here, we study the dynamic response of single-electron tunneling (SET) in a single quantum dot in the few-electron limit upon pulsed and continuous microwave radiation generated by microwave spectrometers. We first characterize the dot by DC transport spectroscopy, i.e., probing the direct tunnel current and the differential conductance. Under microwave excitation, we monitor the direct tunnel current and compare it to that without microwave excitation. Furthermore, the amplitude and phase of the alternating tunnel current induced by microwave radiation (photoconductance) are determined by using a lock-in amplifier.

The quantum dot (Fig. 1(a)) used in this particular experiment is realized in an $Al_xGa_{1-x}As/GaAs$ heterostructure by patterning the surface with Schottky gates. The two-dimensional electron system (2DES) is 90 nm below the surface and has an electron density of $1.7\times10^{15}\,m^{-2}$ and an electron mobility of $80\,m^2/V\,s$. A quantum dot with a radius around 100 nm is formed. The operating temperature of the $^3He/^4He$ bath in the dilution refrigerator is 35 mK, while the electron temperature in these measurements remains at about $T=150$ mK under irradiation with the spectrometer.

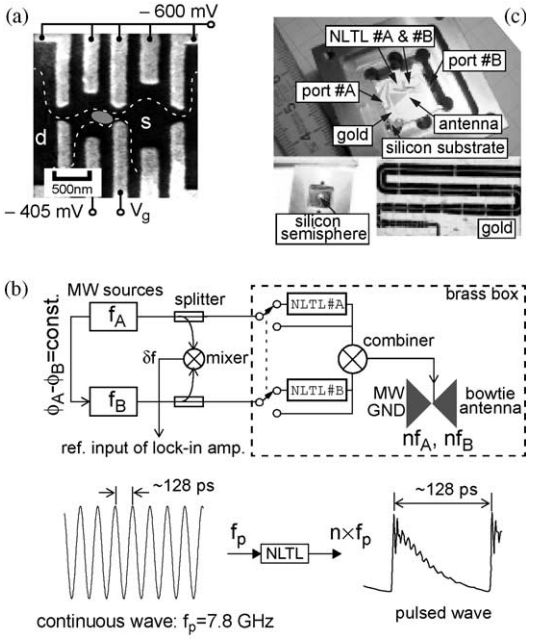

Fig. 1. (a) A single quantum dot is formed by Schottky gates. (b) Schematic diagram of the spectrometer. With NLTLs connected in the circuit, pulsed microwaves can be generated. A continuous flux of microwave photons can be generated with NLTLs disconnected, as described in detail in Ref. [9]. (c) Top view of the heterodyne spectrometer circuit in a brass box with two coaxial connectors feeding the two NLTLs.

The circuit of the spectrometer is schematically shown in Fig. 1(b). At the heart of this spectrometer, two nonlinear transmission lines (NLTLs) are fed with two highly accurate, phase-locked microwave synthesizers (HP 83711A, $f_A\approx f_B=f_p=7.8$ GHz, $\delta f=f_B-f_A\equiv21$ Hz). In contrast to an earlier version [11] we have integrated the spectrometer in a single brass box (Fig. 1(c)), which is mounted in situ on a cylindrical waveguide of the sample holder in the dilution refrigerator at room temperature. Trains of short pulses with harmonic frequency contents ($f_n\approx n\times f_p$) beyond 400 GHz are generated by NLTLs [12]. The NLTLs' outputs are then combined and sent to a planar bowtie antenna (Fig. 1(b)). The power combiner and antenna circuit are defined by evaporating gold onto a high-resistivity silicon substrate (Fig. 1(c)). The superimposed pulse trains of the NLTLs are radiated into the cylindrical waveguide through a silicon hemisphere attached to the antenna on the back side of the circuit (Fig. 1(c)) [13]. The waveguide has a lower cutoff ~80 GHz, and the infrared radiation is blocked by a black polyethylene window. Although the output power of the spectrometer is low to minimize heating, we observe a well-pronounced photoconductance signal. Using a digital lock-in amplifier, we are able to probe the amplitude and phase of the photoconductance in a wideband from 80 to 400 GHz ($10\leq n\leq50$), corresponding to energies of 0.3–1.6 meV, which is comparable to the charging energy and the mean level spacing of the dot (see below). It is particularly important to note that since we filter the induced photocurrent spectrum with a lock-in amplifier, we can perform broadband spectroscopy on the dot under a constant thermal load, in contrast to conventional tuned sources, such as Gunn diodes, whose power variation with frequency complicates broadband measurements. Without NLTLs, two phase-locked

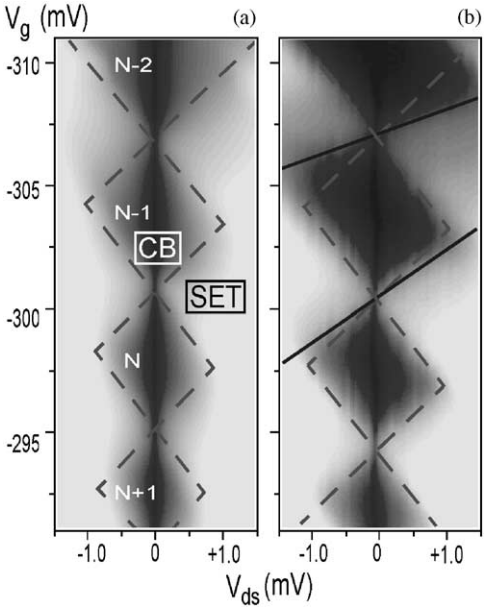

Fig. 2. (a) Logarithmic plot of I_{ds} in the plane of $V_{ds} - V_g$ (gray: $I_{ds} \geqslant 3$ nA, black: $I_{ds} \leqslant 1$ pA). The dashed lines for the enclosed diamonds are obtained from the conductance (otherwise not shown), where the diamond boundaries are better resolved. The number of electrons in the dot is indicated by $N+1$, N, $N-1$, etc. (b) Logarithmic plot of I_{ds} measured under pulsed microwave radiation (gray: $I_{ds} \geqslant 0.7$ nA, black: $I_{ds} \leqslant 0.1$ pA). The dashed diamonds are the same as those in (a). The solid lines indicate the actual diamond boundaries.

microwave sources are combined to generate a continuous microwave flux for spectroscopy on a similar single quantum dot [9].

We measure both the direct tunnel current (I_{ds}) and the differential conductance ($g = dI_{ds}/dV_{ds}$) of the dot. In Fig. 2(a), the direct tunnel current is plotted in a linear grayscale presentation. The dashed lines obtained from the conductance measurement reveal Coulomb-blockade (CB) diamonds. Within the diamonds, electron transport is blocked by the charging energy $E_C = e^2/2C_\Sigma$,[1] according to the "orthodox model" of Coulomb blockade [14]. The tunnel barrier connecting the dot with the source contact (thus source-related) is tuned to be less opaque than the drain-related barrier, i.e., $\Gamma_d < \Gamma_s$, as schematically shown in the

[1] The charging energy $E_C = e^2/2C_\Sigma$ is required to add an additional electron onto a quantum dot with a total capacitance C_Σ.

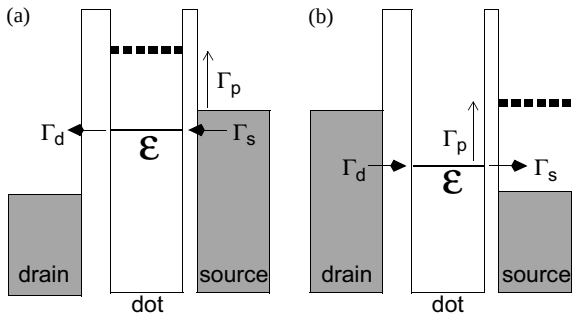

Fig. 3. (a) At positive drain-source bias, the effective electron number in the dot is increased by pumping electrons into the dot. (b) At negative drain-source bias, the effective electron number in the dot is reduced by pumping electrons out of the dot.

level diagrams in Fig. 3. Consequently, the upper-right and the lower-left Coulomb diamond boundaries (along which the dot energy is aligned with the chemical potential in the drain, thus drain-related) are sharper and higher than the upper-left and the lower-right source-related boundaries. The varying size of the diamonds indicates that the dot's total capacitance ($C_\Sigma = C_d + C_s + C_g$) changes upon adding or removing single electrons in the few-electron limit. The capacitance of the dot to the drain ($C_d \approx 98$ aF) and source ($C_s \approx 67$ aF) lead and to the gate ($C_g \approx 25$ aF) are denoted, respectively. We estimate an average charging energy of $E_C \approx 0.4$ meV for the two Coulomb-blockade diamonds from $V_g = -307.5$ to -295 mV (Fig. 2(a)). The drain- and source-related slopes of the diamond are $s_1 = \delta V_g/\delta V_{ds} = 1 + C_s/C_g = 3.66$ and $s_2 = \delta V_g/\delta V_{ds} = -C_d/C_g = -3.93$, respectively. The slopes yield a scaling factor $\alpha = C_g/C_\Sigma = 1.3 \times 10^{-1}$ that relates the gate voltage (V_g) to an energy scale ($\Delta E = -e\alpha\Delta V_g$). Although no DC transport through excited states is resolved in the SET regime (Fig. 2(a)), we determine the mean level spacing of the dot $\Delta\varepsilon^* \approx 200$ μeV using photoconductance measurements under pulsed microwave radiation (see below).

Pulsed microwave radiation changes the slopes of the diamond boundaries in Fig. 2(b) compared to those in Fig. 2(a). We find that the drain-related slope s_1 is decreased to 3.30, and the source-related slope s_2 to about -0.45 (corresponding to the

upper-most diamond in Fig. 2(b)). Taking the "orthodox model", the tunnel barrier capacitances C_d and C_s are reduced by 89% and 18%, respectively. The reduction of C_g is only 3%.[2] Although the slopes under higher gate voltages are closer to the ones in the DC limit, the capacitance of the drain-related barrier C_d maintains a clearly different response under pulsed radiation.

This reduction in slopes arises from the fast pumping by pulsed microwave radiation. For the source-related resonance under a positive bias, the level diagram can be illustrated as in Fig. 3(a). Without microwave radiation, electrons tunnel into the ground state from the source lead at a rate of Γ_s and escape out of the dot at a rate of Γ_d. The total tunneling rate through the dot is found $\Gamma_d\Gamma_s/(\Gamma_d+\Gamma_s)<4\,\mathrm{GHz}$. When pulsed microwave radiation is present, electrons in the source lead are excited and pumped into excited or virtual states in the dot at a rate of about $\Gamma_p = f_p$. Since the $\Gamma_d < 8\,\mathrm{GHz} < \Gamma_s$ and then $\Gamma_d < \Gamma_p$, the average electron number $\langle N\rangle \propto \Gamma_d\Gamma_s/(\Gamma_d+\Gamma_s)$ in the dot is increased compared to the static value. This increase in the electron number $\delta\langle N\rangle$ results in an upward shift of each quantum state $\delta E = e^2\delta\langle N\rangle/C_\Sigma$. Furthermore, it is expected that $\delta\langle N\rangle$ increases with V_{ds} since Γ_s becomes larger and larger compared to Γ_d. Correspondingly, a downward shift of gate voltage $\delta V_g = -e\delta\langle N\rangle/C_g$ is required to match the original position of the resonance, i.e., the diamonds' slopes are reduced. Similarly, the average electron number in the dot is reduced in the case with a negative bias under radiation (Fig. 3(b)), which requires a higher gate voltage to compensate the downward energy shift. In turn, the slopes are reduced as well. Hence, the slope change observed reflects the dynamic pumping of electrons by pulsed radiation and the connected relaxation processes which can be characterized by the electron's dwell time in the dot. Furthermore, since the source-related tunnel barrier is more transparent than the drain-related one and the dot can be filled or emptied by electrons from the source, the drain-related resonance experiences a smaller change by pulsed excitation. By varying the pulse repetition rate f_p and measuring the slope change, it is possible to obtain the tunneling rates through the tunnel barriers. In contrast, earlier work on a similar single quantum dot [9] showed that the slopes of the diamond boundaries are not shifted when the applied microwave radiation is continuous rather than pulsed.

In the absence of microwave radiation, hardly any fine structure indicating electron transmission through excited states is found in the SET regime (Fig. 2(a)). As the dot is strongly coupled to the contacts, strong inelastic tunneling at finite bias masks tunneling peaks from excited states. Under pulsed radiation, since the spectrometer emits about 40 harmonics of the fundamental microwave frequency simultaneously, possible sidebands from photon-assisted tunneling (PAT) are extensively overlapped. We can, however, select or filter the dot's response to a given harmonic using a phase-sensitive detection method, given the linear response, which we verify by checking the dot's proportional response to slight changes in spectrometer power [11]. The dual-source spectrometer as shown in Fig. 1(b) allows us to probe the response at different harmonics. The spectrometer emits picosecond pulses that have a beat frequency $f_{bn} = n\times\delta f$ (Fig. 1(d)), since it is driven by two phase-locked synthesizers with $f_{A,B}\approx f_p = 7.8\,\mathrm{GHz}$ offset by $\delta f \equiv 21\,\mathrm{Hz}$. This allows filtering of the dot's response at harmonics (f_n) with a digital lock-in amplifier whose base reference is δf. With a two-channel lock-in amplifier we are able to monitor the complex in-phase and out-of-phase (X and Y) components of the photoconductance resulting from the corresponding millimeter-wave harmonics (f_n).

Thus, in contrast to the total-induced current under radiation of Fig. 2(b), two photoconductance spectra (of the Y component)[3] taken at the 12th harmonic of the beat frequency ($f_{12} = 93.6\,\mathrm{GHz}$ (a)) and the 18th harmonic

[2] This small reduction in gate capacitance indicates that the microwave field induces only slight changes in the size of the quantum dot and in the capacitances connecting to the drain and source contacts. However, the tunneling rates can be varied greatly.

[3] The Y component reveals features similar to the X component and the amplitude $A = \sqrt{X^2+Y^2}$, but in this case had better resolution.

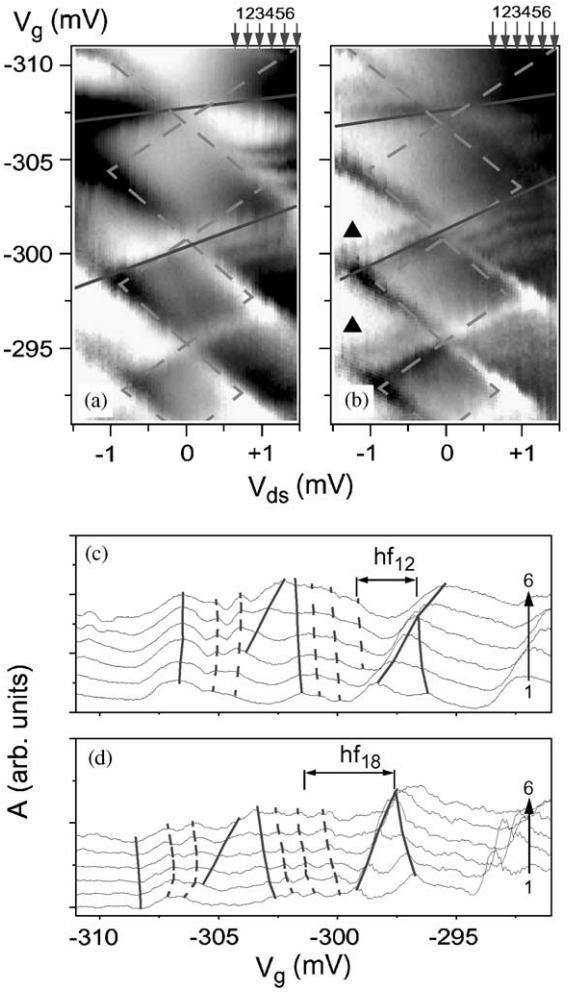

Fig. 4. Linear plot of the Y component of the high-frequency conductance at the 12th (a) and 18th (b) harmonic ($f_{12} = 93.6\,\mathrm{GHz}$, $f_{18} = 140.4\,\mathrm{GHz}$). The plotted data is in arbitrary units: White represents negative values and black is positive. In (a) and (b), the dashed lines indicate the diamonds as shown in Fig. 2 (a). The solid lines show the actual diamond boundaries. Two solid triangles mark resonances from excited states of the dot under negative bias. In (c) and (d), the blue solid lines trace the ground-state resonances, while the dashed lines represent the excited-state resonances as shown in (a) and (b). The traces in (c) and (d) are extracted from (a) and (b) at six specific gate voltages, respectively.

($f_{18} = 140.4\,\mathrm{GHz}$ (b)) are given in Fig. 4. The diamond-shaped Coulomb-blockade regions resemble those observed in Fig. 2(b), i.e., slopes of the diamond boundaries are reduced. Furthermore, additional features are observed in the SET regime. We extract single traces from Fig. 4(a) and (b), as shown in Fig. 4(c) and (d), respectively. The solid lines indicate the ground-state resonances corresponding to the CB diamond boundaries in Fig. 4(a) and (b). The dashed lines reveal fine structure from excited-state resonances in the SET region.[4] We find the mean level spacing $\Delta\varepsilon^* \approx 200\,\mu\mathrm{eV}$. The ability to resolve excited states under pulsed microwave excitation benefits from the fact that only the response of a single harmonic is detected by the lock-in amplifier.

The phase signal obtained reflects the sign change of the photon-induced tunnel current (otherwise not shown). In general, when the time scale of the slowest tunneling process is comparable to the offset frequency δf, it is possible to deduce this time scale from the phase signal. As studied in Ref. [9], when a continuous microwave flux is applied the phase signal reflects the slow charge relaxation processes between the excited and ground states in the dot.

In summary, we used a pulsed microwave spectrometer for probing the dynamics of electrons confined in quantum dots. We found deviations of the dot's capacitances under pulsed excitation compared to the equilibrium values, a signature of the effective relaxation times of single-electron tunneling. This setup also allows us to determine the high-frequency conductance in a wideband fashion similar to the quasi-static limit. We observed excited electron states in the quantum dot at finite bias, which are otherwise not observable in the absence of microwave excitation.

We would like to thank J.P. Kotthaus and K. von Klitzing for continuous support and discussion. This work has been supported by the Deutsche Forschungsgemeinschaft and DARPA

[4] We find that the fine structures observed with positive drain-source bias depend weakly on the harmonic at which the photoconductance is detected. Hence, we tend to take the fine structures as transport through excited states but not PAT sidebands. Although PAT sidebands are weakly evident at positive bias, we do observe stronger frequency-dependent features at negative drain-source bias, such as two excited-state resonances at the 18th harmonic (marked by solid triangles in Fig. 4(b)), while these resonances are not found at the 12th harmonic in the SET regime (Fig. 4a)).

(Ultrafast Electronics Program). H.Q. acknowledges support by the Volkswagen foundation, R.H.B. thanks the Alexander von Humboldt Stiftung for the Feodor-Lynen stipend and we also thank the Office of Naval Research and the National Science Foundation (PECASE program for D.v.d.W.) for support. This work was supported in part by the National Security Agency (NSA) and Advanced Research and Development Activity (ARDA) under the Army Research Office (ARO).

References

[1] D. Loss, D.P. DiVincenzo, Phys. Rev. A 57 (1998) 120.
[2] V.I. Kozub, A.M. Rudin, Phys. Rev. B 49 (1994) 5710.
[3] R. Aguado, L.P. Kouwenhoven, Phys. Rev. Lett. 84 (2000) 1986.
[4] S. Komiyama, O. Astafiev, V. Antonov, T. Kutsuwa, H. Hirai, Nature 403 (2000) 405.
[5] T.H. Oosterkamp, T. Fujisawa, W.G. van der Wiel, K. Ishibashi, R.V. Hijman, S. Tarucha, L.P. Kouwenhoven, Nature 395 (1998) 873.
[6] H. Qin, A.W. Holleitner, K. Eberl, R.H. Blick, Phys. Rev. B Rap. Commun, (2001), in press, cond-mat/0011155.
[7] T. Brandes, F. Renzoni, R.H. Blick, Phys. Rev. B 64 (2001) 035319.
[8] Y. Nakamura, Yu A. Pashkin, J.S. Tsai, Nature 398 (1999) 786.
[9] H. Qin, F. Simmel, R.H. Blick, J.P. Kotthaus, W. Wegscheider, M. Bichler, Phys. Rev. B 63 (2001) 35320.
[10] T. Fujisawa, Y. Tokura, Y. Hirayama, Phys. Rev. B 63 (2001) 81304.
[11] R.H. Blick, D.W. van der Weide, R.J. Haug, K. Eberl, Phys. Rev. Lett. 81 (689) 1998.
[12] D.W. van der Weide, F. Keilman, US Patent 5,748,309, May 5 1998.
[13] D.W. van der Weide, J. Opt. Soc. B 11 (2553) 1994.
[14] H. Grabert, M.H. Devoret (Eds.), Single Charge Tunneling: Coulomb Blockade Phenomena in Nanostructures, Series B: Physics, NATO Advanced Study Institute, Vol. 294, Plenum, New York, 1992.